
PERGAMON

Journal of Quantitative Spectroscopy & Radiative Transfer 71 (2001) 237–247

Journal of Quantitative Spectroscopy & Radiative Transfer

www.elsevier.com/locate/jqsrt

Detailed hydrodynamic and X-ray spectroscopic analysis of a laser-produced rapidly-expanding aluminium plasma

D.M. Chambers[a,*], S.H. Glenzer[b], J. Hawreliak[c], E. Wolfrum[c], A. Gouveia[c], R.W. Lee[b], R.S. Marjoribanks[d], O. Renner[e], P. Sondhauss[c], S. Topping[f], P.E. Young[b], P.A. Pinto[a], J.S. Wark[c]

[a] *Steward Observatory, University of Arizona, Tucson, Arizona, AZ 85721, USA*
[b] *Lawrence Livermore National Laboratory, P.O. Box 808, Livermore, CA 94551, USA*
[c] *Department of Physics, Clarendon Laboratory, University of Oxford, Parks Road, Oxford OX1 3PU, UK*
[d] *Department of Physics, McLennan Physical Labs, University of Toronto, 60 St. George Street, Toronto, Ontario, Canada M5S 1A7*
[e] *Institute of Physics, Czech Academy of Sciences, 18221 Prague, Czech Republic*
[f] *School of Mathematics and Physics, Queens University Belfast, Belfast BT7 1NN, UK*

Abstract

We present a detailed analysis of K-shell emission from laser-produced rapidly-expanding Al plasmas. This work forms part of a series of experiments performed at the Vulcan laser facility of the Rutherford Appleton Laboratory, UK. 1-D planar expansion was obtained by over-illuminating Al-microdot targets supported on CH plastic foils. The small size of the Al-plasma ensured high spatial and frequency resolution of the spectra, obtained with a single crystal spectrometer, two vertical dispersion variant double crystal spectrometers, and a vertical dispersion variant Johann Spectrometer. The hydrodynamic properties of the plasma were measured independently by spatially and temporally resolved Thomson scattering, utilizing a 4ω probe beam. This enabled sub- and super-critical densities to be probed relative to the 1ω heater beams. The deduced plasma hydrodynamic conditions are compared with those generated from the 1-D hydro-code Medusa, and the significant differences found in the electron temperature discussed. Synthetic spectra generated from the detailed term collisional radiative non-LTE atomic physics code Fly are compared with the experimental spectra for the measured hydrodynamic parameters, and for those taken from Medusa. Excellent agreement is only found for both the H- and He-like Al series when careful account is taken of the temporal evolution of the electron temperature. © 2001 Published by Elsevier Science Ltd.

* Corresponding author.
E-mail address: chambers13@llnl.gov (D.M. Chambers).

0022-4073/01/$ - see front matter © 2001 Published by Elsevier Science Ltd.
PII: S0022-4073(01)00071-1

1. Introduction

The work presented here forms part of an ongoing project aimed at studying the effects of velocity gradients on the ionization balance, and spectral emission from, laser produced plasmas. Previous work has shown the necessity of taking into account the velocity gradient when calculating the spectral emission from optically thick lines [1–4]. More recent work has concentrated on laser produced aluminium plasmas, and specifically on the line shape of the Ly-α transition [5–8] from hydrogenic ions. For a static hydrogenic Al-plasma the doublet nature of the $n=2$ energy level is reflected in a doublet line shape, with a 2–1 intensity ratio between the emission from the $2p_{3/2}$ and $2p_{1/2}$ to the $1s_{1/2}$ ground state transitions. The effect of the velocity gradient on this transition was studied in detail in cylindrical geometry by Patel et al. [8]. They observed a single emitted line rather than a doublet, when observing along the plasma expansion direction. They used 1-D hydrocode simulations and a relatively simple radiation transfer routine to model the Ly-α emission. Good agreement was found between the experiment and simulations, enabling the pertinent physical effects to be highlighted. The emission profile of the $2p_{3/2}$–$1s_{1/2}$ transition, when emitted from the slowly moving plasma region close to the target surface, was Doppler shifted into resonance with the absorption profile of the $2p_{3/2}$–$1s_{1/2}$ transition further out in the plasma where the plasma velocity was much higher. Simulations also showed that the single line recorded was therefore emitted primarily by the supposedly weaker $2p_{3/2}$–$1s_{1/2}$ transition. This highlights the importance of a large velocity gradient, as opposed to simply a large velocity, as it is the different motions of the plasma at different positions that create these spectral overlaps.

There has been interest in this work from the astrophysical community as several astrophysical phenomena have large velocity gradients present, such as supernovae and accretion disks. Whilst the laser-plasma experiments are on a vastly different scale, the pertinent physics in the radiation transport problem within these different regimes is essentially the same. These laboratory experiments therefore represent an opportunity to provide a simple benchmark, for the radiation transfer simulations used to model these large-scale astrophysical phenomena. The laboratory plasma hydrodynamic conditions can be independently measured, providing all the necessary information to isolate the radiation transfer problem in the calculation. It should be noted that the laboratory experiment also provides a situation that is vastly simplified from that of the astrophysical one. The laser produced Al-plasma creates a spectral overlap of the two sub levels of the Ly-α transition, whereas thousands of overlapping lines could be present in the case of a supernova. This benchmark would therefore be in no way complete but would represent a very important first step in testing the basic ability of these codes.

In order to model the spectral emission from such a rapidly expanding plasma, it has been usual to rely on simulations to provide the necessary spatially and temporally varying plasma hydrodynamic and atomic kinetic conditions. One of the goals of this project is to move away from the reliance on hydrodynamic simulations and to measure these parameters experimentally, and by methods that are independent from the X-ray spectroscopy. This should not only enhance the credibility of any subsequent radiative transfer calculation, but also provide useful information on the level of accuracy of the 1-D hydrodynamic simulations, and when they can, or cannot, be relied upon.

To this end a range of diagnostic techniques have been employed to measure as many parameters of the plasma as possible. These include Thomson scattering, K-shell spectroscopy, pinhole imaging, and shadowgraphy. To enhance the power of these techniques in accurately diagnosing the plasma conditions the experimental geometry was designed to create, as near as possible, a one-dimensionally expanding Al-plasma. This also has the advantage of improving the ability of hydrodynamic simulations to accurately predict the plasma conditions.

2. Experimental arrangement

The experiments were carried out using the VULCAN laser at the Central Laser Facility of the Rutherford Appleton Laboratory, UK. Thin foil targets were illuminated with six beams of the Vulcan laser giving ~ 900 J of IR energy in a 1 ns (FWHM) trapezoidal pulse. Each laser beam was smoothed using a random phase plate (RPP), giving a uniform energy density 500 μm diameter focal spot at the target surface. All six focal spots were then overlaid producing an intensity at the target of 3.5×10^{14} W cm^{-2}. The targets consisted of an aluminium microdot, 200 μm × 200 μm square and 1 μm thick, coated onto a 6 μm plastic (paralyenen, C_8H_8) foil held between two jaws 3 mm apart, as shown in Fig. 1. This target and laser arrangement ensured a 1-D Al-plasma expansion; the Al-plasma was confined by the plastic plasma on all sides created by the over-illumination of the Al microdot.

The hydrodynamic properties of the plasma were measured by monitoring the Thomson scattering [9,10] of a further beam from the Vulcan laser. This beam was frequency quadrupled to 263 nm, and focused using a 1 m focal length lens into the plasma at 90° to the plasma expansion direction. The distance from the target surface was then varied to allow different temporally evolving density regions to be accessed. This beam line provided up to 50 J at the 4ω frequency and had a 2 ns pulse length. The longer pulse length enabled the plasma to be probed not only during the 1 ns heater pulse duration, but also for the following 1 ns as the plasma expanded and cooled. The scattered 4ω radiation was collected along the plasma expansion direction using an $f/10$ lens and measured using a 1 m spectrometer, incorporating a 3600 l/mm grating, coupled to an Imacon 500 streak camera. The Thomson ion feature could then be resolved at all times of the probe beam allowing the temporal evolution of the electron temperature, the electron density, and the plasma expansion velocity to be determined.

A further 2ω, 2 ns, probe beam was used to create shadowgram images of the expanding plasma. This beam was collimated to have a 1 cm diameter, and passed through the target perpendicular to both the expanding plasma and to the Thomson probe beam. The plasma was magnified ($\times 5$) using an $f/5$ lens onto a Kentech gated optical imager (GOI), which took 100 ps snap shots images at 0.5, 1.0 and 1.5 ns after the start of the heater pulses on each shot. The expansion of the plasma could then be seen directly from the growth of the shadow in the three consecutive images. This also provided further information concerning the electron density for the Thomson data, which otherwise would have been solely inferred from absolute intensity measurements of the ion feature (note the Thomson electron feature was not recorded in these experiments).

K-shell emission from the Al-plasma was recorded using a single crystal spectrometer (SCS), two vertical dispersion variant, double crystal spectrometers (DCV) [11] and a vertical

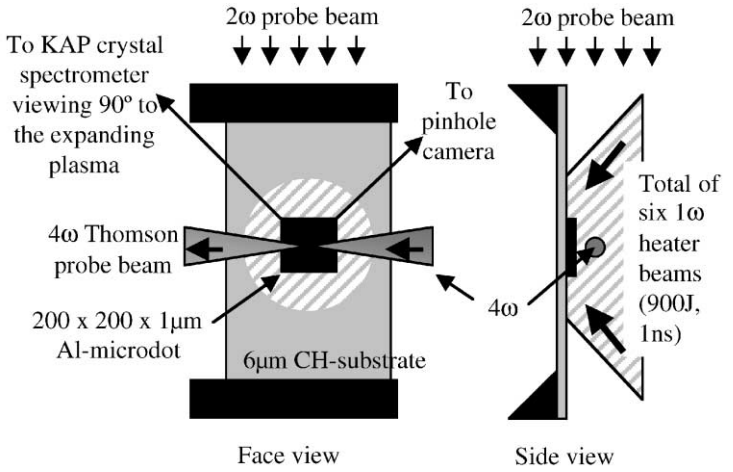

Fig. 1. A schematic diagram of the target in both face on and side views. A 1 mm wide, 6 μm thick, CH foil is held between two jaws 3 mm apart. Centered on the CH foil is an Al microdot, this dot is illuminated by six arms of the Vulcan laser in a 500 μm diameter focal spot.

dispersion variant Johann crystal spectrometer (VJS) [12]. The SCS incorporated a KAP (potassium hydrogen phthalate) crystal cleaved on the 1 0 0 plane, the DCV's each contained two ADP (ammonium dihydrogen phosphate—1 0 1) crystals and the VJS a cylindrically curved quartz (1 0 0) crystal. The DCV's were mounted on a 26 cm diameter ring: the microdot target was positioned in the center of this ring to better than 50 μm. This allowed the spectrometers to be positioned at various angles with respect to the plasma expansion direction to measure the angular effects on the spectral line profile of the Ly-α line. The effect of the velocity gradient in the plasma on the line profile could then be studied, since for each angle of emission the radiation travels through a hydrodynamically different set of plasma conditions. The VJS was positioned at 90° to the expanding plasma, and spatially and spectrally resolved the Ly-α, Ly-β and higher n transitions on a series of shots. The higher luminosity of the VJS over the DCV's allowed weaker emission to be measured from further out from the target surface. However, the VJS was only used on some shots, as it was not possible to run the Thomson probe beam at the same time due to geometrical constraints. Further studies of these line profiles, from both the DCV's and the VJS have not yet taken place, and thus this part of the project will not be discussed further here, but will be presented in a future publication.

The SCS provided a broader spectral coverage than the DCV's, between 6.8 and 5.4 Å. This range includes six primary K-shell spectral lines from hydrogenic and helium-like aluminium; these are Ly-β, Ly-γ, Ly-δ, He-β, He-γ, and He-δ. The spectrometer was positioned in the plane of the target and utilized a 15 μm slit so as to spatially resolve the expanding plasma with a magnification of 3. The Thomson probe beam prevented looking side on to the microdot targets with the SCS, so the spectrometer was positioned at an angle of 45° with respect to the orientation of the microdot, see Fig. 1. The spectra were recorded on a 16 bit Andor CCD camera. Fig. 2 shows a typical spectra as recorded by the 16 bit CCD. All six primary lines are easily resolved, and the spectral line intensities were reproducible on a shot to shot basis to

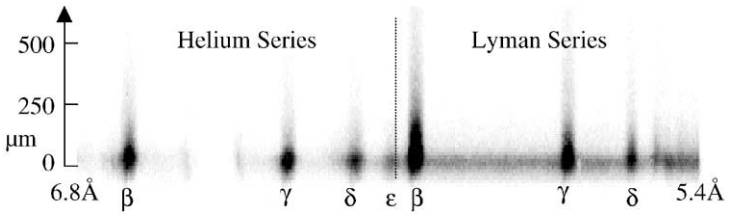

Fig. 2. The spatially resolved Al K-shell spectra as recorded by the KAP single crystal spectrometer. The hydrogenic and helium-like emission lines can clearly be identified.

the 5% level. The spectral width of the lines recorded with the SCS was due entirely to source broadening.

3. Comparison of measured hydrodynamic conditions with 1-D simulations

Before turning our attention to the emission spectra it is of interest to compare the measured and simulated hydrodynamic conditions. In the experiment, we have tried to create a 1-D Al-plasma expansion. This was to enable 1-D hydrodynamic simulations to be used with some degree of confidence to predict the plasma conditions. If the plasma was not 1-D then modeling using a 1-D hydrocode would be inappropriate, and discrepancies between the measured and simulated conditions expected. Fig. 3(a) and (b) show the plasma expansion from an Al microdot mounted on a CH foil target. Fig. 3(a) shows a time integrated pinhole image at 90° the expanding Al emission, no emission is seen from the CH plasma. The image is taken at 45° in the vertical plain so the microdot is seen from the corner giving a dot full width of 280 μm. Here, the Al expansion can clearly be seen to be linear, as there is no lateral expansion of the Al for distances $\leqslant 250$ μm from the target surface. Fig. 3(b) shows a 2ω (527 nm), 100 ps gated shadowmetric image taken at 0.5 ns after the start of the heater pulse, again at 90° to the expanding plasma. The dimensions of the original Al microdot, laser focal spot and CH foil are marked in the diagram. Here the total plasma emission can be seen to be hemispherical. The bright spot in the center can be attributed to self-emission at the 2ω frequency from the Al-plasma. This bright region again shows the linear expansion of the Al-plasma, with no emission seen from the CH regions.

Fig. 3(a) shows that the desired 1-D expansion of the Al-plasma has been achieved at least for those regions corresponding to strong X-ray emission. This allows us to assume that a cross-section through the Al-plasma, perpendicular to the expansion direction, would reveal a constant density and temperature across it at any given time. We would therefore expect the use of a 1-D hydrodynamic simulation to be applicable, in trying to reproduce the plasma conditions to a reasonable degree of accuracy. However, looking at Fig. 3(b) it is clear that this 1-D Al-plasma sits within a 3-D hemispherically expanding CH plasma. The effects of this will not be taken into account in the 1-D planar simulations.

Fig. 4(a) shows both the measured and simulated electron temperature at the end of the heater pulse as a function of distance from the target for the Al-plasma. A 1-D planar geometry hydrodynamic simulation using the code Medusa [13,14] (solid line) is compared with

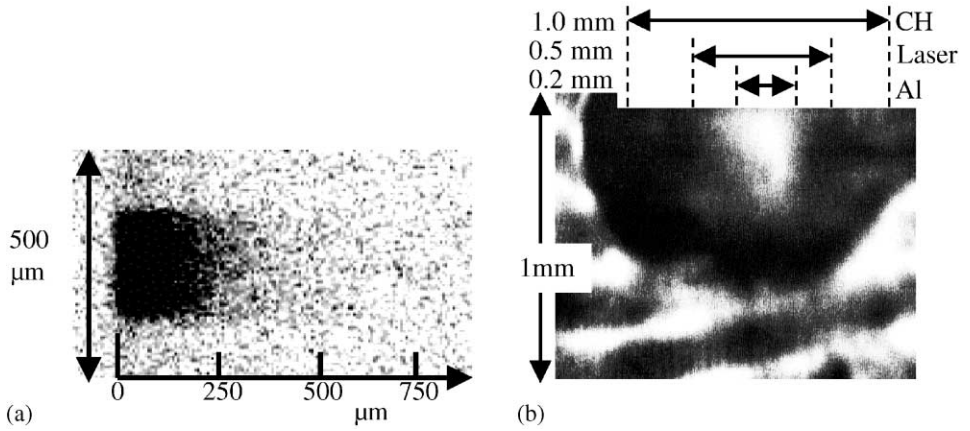

Fig. 3. A X-ray pinhole (a) and an optical (2ω) 100 ps gated shadowgram image (b) both taken at 90° to the plasma expansion direction. (b) also shows the original widths of the CH foil, the laser focal spot and the Al microdot. The white area at the top of the image represents the region blocked by the target mount.

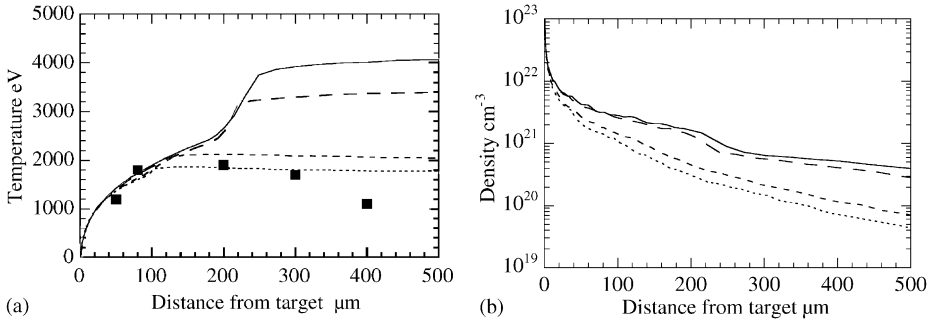

Fig. 4. Electron temperature (a) and electron density (b) profiles at the end of the heater pulses as a function of distance from the original target surface. The lines represent different 1-D Medusa simulations, planar geometry (solid), and spherically symmetric with various diameter spheres 5 mm (large dashes), 500 μm (small dashes) and 320 μm (dots). Also shown are the experimentally measured electron temperatures from Thomson scattering (squares).

that measured from Thomson scattering in the experiment. The detailed analysis of the Thomson scattering measurements are not presented here, but the methodology employed can be found in the paper by Hawreliak et al. [13,14]. Up to 100 μm from the target surface fairly in good agreement can be seen, however, at larger distances there are considerable differences, with Medusa predicting a temperature profile far in excess of that actually measured. One possible explanation for this might be thought to be a deviation from a linear expansion of the plasma, where lateral expansion would cause extra cooling in the experiment. Though as seen in Fig. 3(a) and 3(b) there is good reason to believe this is not so, at least for the Al-plasma.

We have, however, seen in Fig. 3(b) that the expansion of the plasma as a whole is indeed laterally expanding. A further possibility therefore presents itself: while no lateral expansion of the Al-plasma exists, the CH plasma is cooled rapidly by this expansion process, and so

the Al-plasma cools by lateral heat transport. It must be noted, however, that another possible explanation could simply be a missing physical process in the electron temperature calculations by Medusa. In order to approximate the effect of cooling by lateral heat transport the Medusa hydrocode was run in a spherically symmetrical geometry. This still provides a 1-D result, but the effects of lateral spreading are taken into account, the results of these simulations are also shown in Fig. 4(a). Three different diameter spheres have been used, 5 mm, 500 μm and 320 μm. The large diameter sphere shows, as one might expect, that at large diameters the simulations in spherical geometry approach the planar geometry results. The other two spheres correspond to the situations where the diameter (500 μm), or the half circumference (320 μm) of the sphere equals the diameter of the experimental laser spot. In the case of the 320 μm diameter sphere, the temperature is indeed reduced sufficiently to match the experimentally measured values. Although this simulation is at best a crude approximation of the hydrodynamics, further results from this particular case will be included for comparison in the following analysis.

We can use the shadowgram images to give an indication of the reliability of the simulations, in either geometry, to predict the electron density. To calculate the electron density surface corresponding to the edge of the dark region in Fig. 3(b) is non-trivial, as the beam refraction by the plasma is a function not only of the density but the density gradient as well. Therefore without knowing the density gradient explicitly it is impossible to calculate the corresponding density from the images independently. However, it is possible to determine if the densities and density gradients from the Medusa simulations are self-consistent with the plasma images recorded by the GOI. The beam refraction by the plasma is given by

$$\frac{\partial\theta}{\partial x_s} = \frac{\partial\varepsilon}{\partial x_p},$$

$$\frac{\mathrm{d}\theta}{\mathrm{d}x_s} = \frac{\mathrm{d}}{\mathrm{d}x_p}\left(1 - \frac{n_e}{n_c}\right)^{1/2} = (1 - \frac{n_e}{n_c})^{-1/2}\ \frac{1}{2n_c}\ \frac{\mathrm{d}n_e}{\mathrm{d}x_p},$$

where θ is the refraction angle (radians), x_s is the length of the plasma, $\partial\varepsilon/\partial\ x_p$ is the gradient of the dielectric constant perpendicular to the probe beam, n_e is the electron density and n_c is the critical density for the probe laser wavelength. Given the $f/5$ collection of the probe laser any rays deflected by greater then 5.7° will not be collected, hence creating the shadow region on the GOI. Using the density gradients from the Medusa planar geometry simulation, the electron density required to reproduce the edge of the shadow region at this distance from the target surface would be $1.7\ (\pm 0.2) \times 10^{20}\ \mathrm{cm}^{-3}$. The simulations predict a density of $1.4 \times 10^{20}\ \mathrm{cm}^{-3}$ for this distance from the target surface, which is fairly in good agreement. Similar agreement is also found for the GOI images taken at later times, showing that the planar simulations are at least self consistent with the shadowgram images. However, using any of the spherical geometry simulations produces a very poor match to the beam refraction seen in the GOI image. A much higher density than predicted by Medusa, for the given density gradients, would be needed to produce the beam refraction measured. Indeed, the smaller the sphere, the worse the match becomes, hence these simulations are not self-consistent with the shadowgram data. This strongly supports the case that the experiment produced a 1-D Al-plasma expansion, and that the Medusa 1-D planar geometry simulations can accurately reproduce the temporal evolution of the electron density.

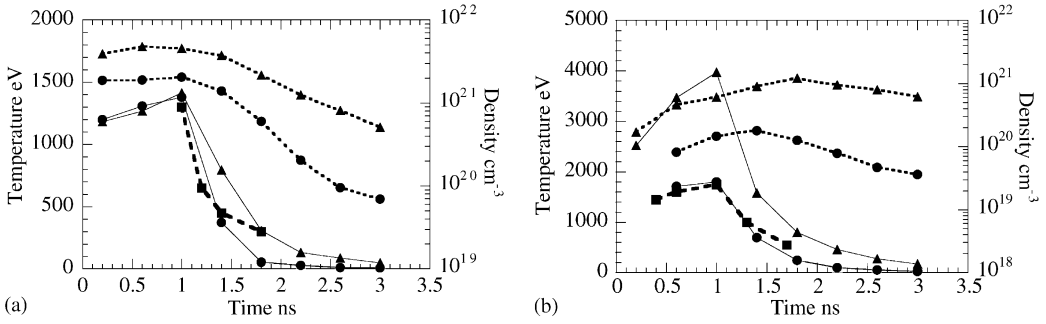

Fig. 5. Electron temperature and electron density time histories at 50 μm (a) and 300 μm (b) from the original target surface. Medusa simulated temperatures (solid lines) and densities (dotted lines) are shown from 1-D planar geometry (triangles) and from a 1-D spherically symmetric geometry using a 320 μm diameter sphere (circles). Also shown are the experimentally measured electron temperatures from Thomson scattering (squares).

Fig. 5 shows the temperatures and densities at 50 and 300 μm from both planar and spherically symmetric simulations (320 μm sphere) and the Thomson scattering measurements as a function of time. The electron density for the spherical and planar geometry simulations can be seen to differ by only a small factor at early times close to the target surface, but by an order of magnitude by the end of the probe pulse. At 300 μm from the target surface the difference in the simulated electron densities can be seen to be large at all times. We would expect the planar geometry density simulations to be more accurate than the spherically symmetric simulations, as the plasma images in Fig. 3 show no signs that the Al-plasma has expanded laterally. This is strongly supported by the planar simulation densities, and density gradients, being self-consistent with the beam refraction seen in the shadowgram images. It is clear that the planar geometry simulations predict an electron temperature far in excess of that measured. The spherically symmetric simulations do produce much better agreement for the electron temperature, but from the images and density information, we know no lateral expansion has occurred to validate such a simulation for the Al-plasma. However, the simulation in spherical geometry would be more applicable to the surrounding CH plasma, which from the shadowgram images can be seen to have expanded considerably laterally, and become hemispherical in nature. It is therefore not unreasonable to expect the temperature of the surrounding CH plasma to have affected that of the Al-plasma, causing the electron temperature to be much lower than that simulated in planar geometry.

4. K-shell spectra

In this section, we will turn our attention to the experimental Al K-shell spectra, and the ability to synthetically reproduce these spectra with the detailed term non-LTE atomic physics code Fly [15]. In order for Fly to generate spectra a series of input parameters are required, these include the atomic number Z, electron temperature, electron density, plasma size (for opacity), the ratio between the ion and electron temperatures and the source broadening function. The ion temperature is set to be half the electron temperature, this is found to be a good approximation

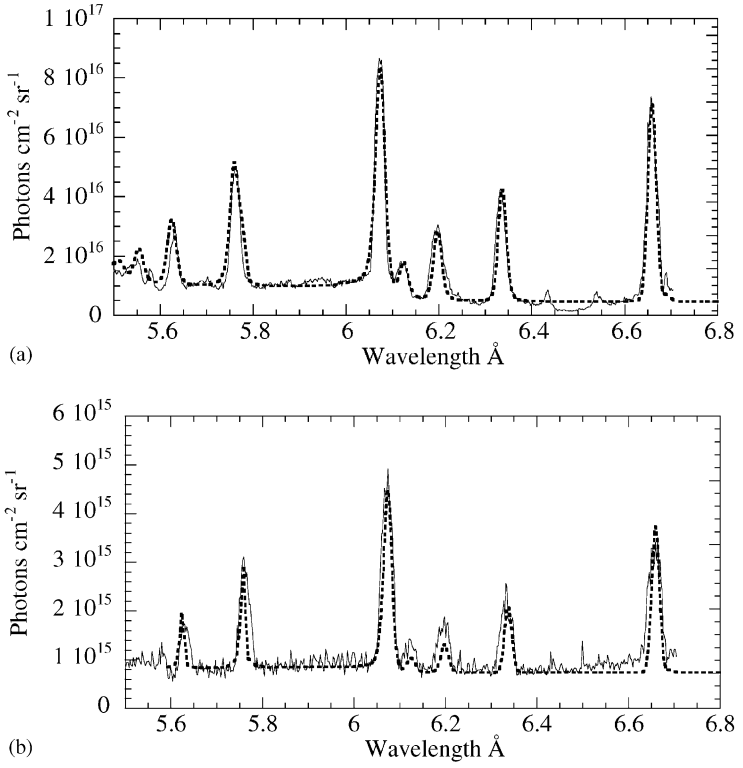

Fig. 6. A comparison between the experimentally measured, spatially resolved, Al k-shell spectra at 50 μm (a) and 300 μm (b) from the target surface. Also shown are synthetic time dependent spectra generated from Fly (dotted lines). Input electron temperatures for Fly are taken from the Thomson scattering measurements, and the densities from the planar geometry Medusa simulations.

from the hydrodynamic simulations for the times when there is significant K-shell emission. Z, the plasma size and the source broadening function (from the Al dot size) are known or can be measured, so the only variables available to alter the synthetic spectra are the electron temperature and density. The electron temperatures used are those measured from Thomson scattering, and the electron densities are those from the 1-D planar geometry Medusa simulations. We study two positions within the plasma in detail, 50 and 300 μm from the original target surface. 50 μm is chosen as it represents the peak in the emission from the Lyman series emission lines. 300 μm is the furthest position from the target surface, where we have confidence that the Al-plasma expansion is 1-D, and at which we have Thomson scattering measurements. Fig. 6 shows the experimentally generated spectra compared with those of Fly for 50 μm (a) and 300 μm (b) from the original target surface. Excellent agreement can be seen for the entire K-shell spectra in both cases. It should be noted that none of the lines of interest are optically thin and the inclusion of the correct plasma size in Fly is vital for reproducing the experimentally generated spectra. To study the effect of opacity a series of different width targets were used, the analysis of the spectra recorded is under way. The results of this analysis will be presented in a future publication.

It is of interest to comment upon the use of different hydrodynamic parameters as inputs for Fly, and on their effect on the spectra generated. Using the 1-D planar geometry temperatures to reproduce the 50 μm spectra produces slight discrepancies in both the Lyman and helium series. These can be attributed to two factors in the temperature profile. Firstly the decrease in temperature after the heater beams turn off is too slow: correcting for this alone produces a near perfect match for the Lyman series emission line. Furthermore, the temperature falls too low late in the pulse: correcting for this matches the helium series. If the spherically symmetric geometry simulation had been used, the better match for the fall off in temperature would have better matched the Lyman series, but the lower late time temperatures enhance the difference in the helium spectra. Using the densities from the spherically symmetric simulation produces a fairly good match to the Lyman series spectra, indicating a low dependence on the density at least to a change of less than a factor of 2. However, the intensity of all the lines in the helium emission series is underestimated compared to the lines in the Lyman series.

At a distance of 300 μm the planar geometry Medusa temperatures are shown to be far too high by the Thomson results, and the corresponding Fly spectra indeed shows the Lyman series dominating over the helium series by more than an order of magnitude. If the densities from the spherical geometry simulation are used, then the relative intensity of the Lyman to helium series emission lines is maintained but the Ly-β and He-β lines are enhanced excessively relative to the rest of the emission lines in each series. This is unsurprising as the reduction in density leads directly to a lower opacity which has a greater affect on the optically thicker Beta lines.

5. Summary and conclusions

In conclusion, we have experimentally generated a planar 1-D, rapidly expanding, Al-plasma. 1-D planar hydrodynamic simulations are shown to predict the electron density profiles of this expansion, but to grossly overestimate the electron temperature. Further, more sophisticated multidimensional simulations would be needed to establish whether this discrepancy is due to the physics within the hydrocode or the presence of the hemispherically expanding CH plasma surrounding the Al. Thomson scattering provides accurate electron temperature measurements from the experiments, allowing temperature and density history profiles to be used in spectral synthesis code Fly. Using the experimentally measured hydrodynamic conditions Fly can reproduce the experimentally generated K-shell Al spectra to a high degree of accuracy. Using the electron temperature profiles predicted by the planar hydrodynamic simulations, or indeed any other hydrodynamic profiles, leads Fly to produce synthetic emission spectra inconsistent with the data. We now, therefore, have confidence in the ability to further use the results from this experimental campaign as a test bed for radiation transfer simulations.

Further work on the hydrodynamic conditions and spectral synthesis is also still underway. We will attempt to confirm the 1-D hydrocode density predictions using the absolute intensities of the Thomson scattering ion feature, the line shapes measured from the VJS spectrometer, and also from further analysis of the shadowmetric measurements. Whilst all indications are that the 1-D hydrocode is producing the correct results for the evolution of the density profile, we believe it is essential to corroborate this before continuing on with the radiation transfer calculations. Also, a series of different width Al microdots have been used to study the effect of

opacity on the K-shell spectra. The analysis of all of these targets and the density measurements are being prepared and will be presented for a forthcoming publication.

Acknowledgements

The authors would like to acknowledge the help and support of the laser and target area staff at the central laser facility of the Rutherford Appleton laboratory. The primary author would also like to thank P.K. Patel for many helpful discussions throughout the course of this work. This project was funded under US DOE Grant No. DESG03-99D-P00297. Work performed by S.H. Glenzer, R.W. Lee and P.E. Young under the auspices of the US Department of Energy by the University of California, Lawrence Livermore National Laboratory under contract no. W-7405 ENG 48. J. Hawreliak and S. Topping acknowledge funding from the UK EPSRC.

References

[1] Mihalas D. Stellar atmospheres. San Francisco: W.H. Freeman and Company, 1978.
[2] Hummer DG, Rybicki GB. Astrophys J 1982;254:767–79.
[3] Rybicki GB. In: Kalkofen W, editor. Methods in radiative transfer. New York: Cambridge University Press, 1984.
[4] Eder DC, Scott HA. JQSRT 1991;45:189–204.
[5] Wark JS, Djaoui A, Rose SJ, He H, Renner O, Missalla T, Foerster E. Phys Rev Lett 1994;72:1826–9.
[6] Wark JS, He H, Renner O, Kopecky M, Foerster E, Missalla T. JQSRT 1994;51:397–406.
[7] Patel PK, Wark JS, Heading DJ, Djaoui A, Rose SJ, Renner O, Hauer A. JQSRT 1997;57:683–94.
[8] Patel PK, Wark JS, Renner O, Djaoui A, Rose SJ, Heading DJ, Hauer A. JQSRT 1997;58:835–44.
[9] Evans DE, Katzenstein J. Rep Prog Phys 1969;32:207–71.
[10] Glenzer SH, Alley WE, Estabrook KG, De Groot JD, Haines M, Hammer JH, Jaddaud J-P, MacGowan BJ, Moody JD, Rozmus W, Suter LJ, Weiland TL, Williams EA. Phys Plasmas 1999;6:2117–28.
[11] Renner O, Kopecky M, Wark JS, He H, Foerster E. Rev Sc Instr 1995;66:3234–43.
[12] Renner O, Missalla T, Sondhauss P, Krousky E, Foerster E, Chenais-Popovics C, Rancu O. Rev Sci Instr 1997;68:2393–403.
[13] Christiansen JP, Ashby DETF, Roberts KV. Comput Phys Commun 1973;7:271–87.
[14] Djaoui A, Rose SJ. J Phys B 1992;25:2745–62.
[15] Lee RW, Larsen JT. JQSRT 1996;56:535–56.